Annals of Work Exposures and Health, 2018, Vol. 62, No. 5, 604–612
doi: 10.1093/annweh/wxy016
Advance Access publication 27 April 2018
Original Article

Original Article

Quantification of Carbon Nanotubes by Raman Analysis

John A. Lynch[1,2], Quinn T. Birch[1], Thomas H. Ridgway[2] and M. Eileen Birch[1]*

[1]Division of Applied Research and Technology, Centers for Disease Control and Prevention, National Institute for Occupational Safety and Health, Cincinnati, OH, USA; [2]Department of Chemistry, University of Cincinnati, Cincinnati, OH, USA

*Author to whom correspondence should be addressed. Tel: +1(513) 841-4298; fax: +1(513) 841-4545; e-mail: mib2@cdc.gov

Submitted 9 December 2016; revised 7 February 2018; editorial decision 8 February 2018; revised version accepted 19 April 2018.

Abstract

The increasing prevalence of carbon nanotubes (CNTs) in manufacturing and research environments, together with the potential exposure risks, necessitates development of reliable and accurate monitoring methods for these materials. We examined quantification of CNTs by two distinct methods based on Raman spectroscopy. First, as measured by the Raman peak intensity of aqueous CNT suspensions, and second, by Raman mapping of air filter surfaces onto which CNTs were collected as aerosols or applied as small-area (0.05 cm^2) deposits. Correlation (R^2 = 0.97) between CNT concentration and Raman scattering intensity for suspensions in cuvettes was found over a concentration range from about 2 to 10 μg/ml, but measurement variance precludes practical determination of a calibration curve. Raman mapping of aerosol sample filter surfaces shows correlation with CNT mass when the surface density is relatively high (R^2 = 0.83 and 0.95 above about 5 μg total mass on filter), while heterogeneity of CNT deposition makes obtaining representative maps of lower density samples difficult. This difficulty can be mitigated by increasing the area mapped relative to the total sample area, improving both precision and the limit of detection (LOD). For small-area deposits, detection of low masses relevant to occupational monitoring can be achieved, with an estimated LOD of about 50 ng.

Keywords: carbon nanotube; exposure assessment; nanomaterials; Raman

Introduction

Carbon nanotubes (CNTs) are nanoscale graphene cylinders with remarkable physical and chemical properties. Common CNT products include single-walled (SWCNT), consisting of a single graphene layer, or multi-walled (MWCNT). Depending on the method of production, they may present different morphologies and aspect ratios, and may contain catalyst impurities. According to their intended use, CNTs may be functionalized and/or incorporated into composite materials. Though often encountered in research and development and small-scale production contexts, industrial CNT production and commercial applications continue to grow (Lux Research, Inc. August 2016; Future Markets,

Inc. January 2016), as does the number of exposed workers.

The nature and extent of the health risks associated with exposure to CNTs are uncertain. However, a fibrous structure, together with resistance to biodegradation, has prompted toxicological studies of CNTs and carbon nanofibers (CNFs). Findings of animal inhalation studies of some types of materials include pulmonary inflammation, fibrosis, cytotoxicity, mutagenesis, and tumor promotion (Lam et al., 2004, , 2006; Shvedova *et al.*, 2008; Ma-Hock *et al.*, 2009; Aschberger *et al.*, df 2010; Porter *et al.*, 2013; van Berlo *et al.*, 2014; Sargent *et al.*, 2014; Rydman *et al.*, 2015). Complicating efforts to quantify the health risks are the myriad forms of CNTs to which exposure may occur. Variances in purity, aspect ratio, number of walls, presence of catalyst, particle structure (e.g. entangled agglomerate versus fiber-like), and functionalization may all, individually or in combination, affect the resultant biological response. The International Agency for Research on Cancer (IARC) categorized one type of MWCNT as possibly carcinogenic to humans (Group 2B). Insufficient evidence exists for other types of MWCNTs and SWCNTs, and these materials were categorized as not classifiable (Group 3) (Grosse *et al.*, 2014; International Agency for Research on Cancer (IARC), 2014). However, there is sufficient evidence to conclude that exposure to CNTs poses some level of health risk, and that methods for reliable and accurate determinations of exposure are needed. The National Institute for Occupational Safety and Health (NIOSH) set a recommended exposure limit (REL) for airborne CNT/CNF materials at 1 μg m^{-1}, determined as elemental carbon (EC) by NIOSH Method 5040 (National Institute for Occupational Safety and Health, 2013).

Occupational exposures to CNTs have been measured by air sample collection, followed by a combination of EC and electron microscopy analyses. EC analysis (Birch and Cary, 1996; National Institute for Occupational Safety and Health, 2003; National Institute for Occupational Safety and Health, 2013; Dahm *et al.*, 2015; Birch, 2016) is an effective method in contexts where the CNT air concentrations are high relative to environmental background, but when air concentrations are low, and/or the product contains amorphous carbon impurities, the EC analysis often cannot distinguish between CNTs and other EC forms (e.g. soot in raw CNT products or from diesel engines). It also gives no information on the structure or morphology of the CNT particles, and it cannot distinguish between CNTs and any graphitic byproducts of nanotube manufacture (Birch and Cary, 1996; National Institute for Occupational Safety and Health, 2003; National Institute for Occupational Safety and Health, 2013; Dahm *et al.*, 2015; Birch, 2016). Transmission electron microscopy (TEM) allows confirmation of CNT presence, and reveals structural information about the sample. However, TEM analysis is costly and labor intensive, and it is difficult to canvas a large enough area of the sample collection filter to be representative, for the purpose of estimating an air concentration (Birch et al., 2016a,b). Efforts to assess exposure using less laborious methods than TEM, such as Raman spectroscopy, were recently advanced (Shin and Chung, 2013; Grafen *et al.*, 2015; Ruedi, 2016; Stacey *et al.*, 2017).

Here we examine the quantification of CNTs by Raman scattering in two distinct contexts. First, Raman analysis of CNTs suspended in aqueous surfactant solutions was examined as a method for estimating the CNT mass concentration. Analysis of CNTs uniformly dispersed in suspension can circumvent difficulties arising from the heterogeneity of solid samples (Dresselhaus *et al.*, 2005; Graf *et al.*, 2007). Analysis of a suspension also facilitates Raman interrogation by much more rapid dissipation of energy away from the CNTs, which are easily degraded (ignited) by excessive excitation. The second approach that we examined for estimating airborne CNTs is by Raman mapping of the surface of a filter sample, collected either as an air sample or by application of a small aliquot of a CNT suspension to the filter media. In the former case, a mapping method has the principal advantage of allowing direct analysis of the sample collection media, without sample preparation steps. By measuring the frequency or proportion of positive CNT measurements in an area, rather than attempting correlate Raman intensity directly with mass, we overcome difficulties in quantitative Raman analysis that can arise from the variance in intensity caused by scattering from non-uniform solid samples. Measurement across a wider area, collecting spectra from many fields of view, reduces variability due to inhomogeneity of the sample deposit, which adversely affects quantification (Shin and Chung, 2013; Stacey *et al.*, 2017). Further, to improve precision and lower the limit of detection (LOD), a smaller collection area can be used, produced either by application of a sample suspension as a well-defined deposit or by aerosol collection as a focused deposit on a filter or substrate. Results of the Raman analyses of CNT suspensions and filter samples are presented in this paper.

Materials and Methods

Baytubes 150HP and Arkema K2 multi-wall CNTs (Bayer Corporation and Arkema Inc., respectively), and 6-Helix single-wall CNTs (Helix Material Solutions, Inc., Richardson, TX, USA) were mixed into an aqueous

surfactant solution. The surfactant used was Pluronic® F-127 (Pl-127) (Sigma). The CNT-surfactant suspensions were sonicated for between 90 min and 3 h at room temperature. After settling (~30 min), the supernatant was collected and the remainder was discarded. Raman measurements on the resulting suspensions were then performed in either methacrylate cuvettes (Perfector, Inc.) or 1.5 mm ID Kimax-51 glass capillary tubes (Kimble-Chase). After adding a suspension, the capillary tube was sealed at the end to prevent leakage. Measurements of Raman scattering in capillary tubes were taken using either an inVia™ Raman Microscope (Renishaw) with a 50 mW, 633 nm laser at 100% power and 5 s integration time, or a B&WTek model BWS415 i-Raman® Miniature Raman Spectrometer and Microscope (B&WTek, Inc., Newark, DE, USA) with a 785-nm laser at 30% power and 10-s integration time. Raman measurements of CNT-surfactant in cuvettes were performed using the same B&WTek BWS415 i-Raman® Miniature Raman Spectrometer and Microscope with a 785 nm laser, but at 100% power and 50-s integration time. Spectra were analyzed with B&WSpec software (B&WTek, Inc.). Raman peak frequency and intensity data were then compared with EC measurements.

Raman mapping was performed on filter samples using an inVia Raman Microscope (Renishaw) with an automatic stage. For these analyses, two MWCNT products were examined: SMW100 (SouthWest NanoTechnologies, Inc. [SWeNT]) and K2 [Arkema, Inc.]). The CNT samples were prepared either by collection of respirable CNT aerosol onto quartz-fiber filters or by application of a 2-µl aliquot of a CNT suspension (in Pluronic F-127 [Sigma]) to a quartz filter portion, as a small spot, using a micropipette (resulting in a deposit area of ~0.05 cm^2). To generate air samples, the materials were aerosolized by a vortex shaking method (Ku *et al.*, 2006) and collected on 25-mm quartz-fiber filters using air sampling cassettes fitted with GK 2.69 BGI cyclones (BGI, Inc., Waltham, MA, USA [currently Mesa Labs, Inc.]). Respirable CNT aerosol was sampled at 4.2 liters per min (lpm) with personal air sampling pumps (Airchek XR5000, SKC Inc., Eighty Four, PA, USA) connected to the sampler outlets. Raman maps were produced by raster scanning a 400 × 400 µm area of the filter surface in 10 µm steps. A 633 nm, 50 mW laser (inVia Raman Microscope [Renishaw]) was used to induce Raman scatter, at 10% power and through a ×50 magnification lens. Signal integration time was 1 s. Mapping data were evaluated by algorithm using a continuous wavelet transform algorithm to identify the graphitic 'D' (~1309 cm^{-1}) and 'G' (~1620 cm^{-1}) peaks over a given signal-to-noise ratio threshold (10, unless otherwise stated) (Zhang *et al.*, 2010; Li *et al.*, 2013; Hoang, 2014). The number of spectra containing CNT peaks in the given area were then compared with the corresponding EC results.

EC was determined by NIOSH Method 5040, based on a thermal-optical method for organic and EC (Birch and Cary, 1996; National Institute for Occupational Safety and Health, 2003; National Institute for Occupational Safety and Health, 2013; Dahm *et al.*, 2015; Birch, 2016). For application to CNTs, the automatic split that is normally used to distinguish the EC and organic carbon (OC) content of a carbonaceous aerosol sample (usually diesel particulate matter by 5040) was not employed. A manual OC–EC split was assigned based on the thermal profiles of the CNT products (National Institute for Occupational Safety and Health, 2013; Dahm *et al.*, 2015; Birch, 2016). To determine EC concentrations for CNT suspension samples, aliquots of 10 µl were applied to pre-cleaned, quartz filter portions (1.5 cm^2) and measured by thermo-optical analysis. Laboratory generated air samples, collected on quartz filters and cut into 1.5 cm^2 portions, were similarly analyzed to determine EC loading.

Results and Discussion

Quantification of CNTs in suspensions by Raman analysis

Figure 1 shows Raman spectra from a series of 1% Pl-127 (aq) suspensions of differing CNT concentration (0–130 µg ml^{-1}), in quartz cuvettes (1 cm pathlength). Both the CNT 'D' (1309 cm^{-1}) and 'G' (~1620 cm^{-1}) bands are visible, but are somewhat overlapped by surfactant peaks (at ~1290 and 1640 cm^{-1}, respectively). The surfactant peak at 1452 cm^{-1} ($–CH_2$) illustrates the dampening effect of CNT absorption, which decreases the peak intensity with increasing CNT concentration. The CNT-related peaks at first supplant the overlapping surfactant peaks, then increase with concentration up to 40 µg/ml, before decreasing at higher concentrations. One strategy for compensating for this non-linearity of response is to compare the CNT concentration with the ratio of a CNT-related peak and a non-CNT-related peak. Examination of the ratio between the 'D' mode CNT peak at 1309 cm^{-1} and surfactant peak at 1452 cm^{-1} reveals a linear correlation with CNT concentration at lower concentrations, but this relationship grows more complex as the CNT concentration (and attendant absorbance) of the suspension increases.

While absorption due to CNTs obscures the relationship between CNT concentration and Raman scattering at higher concentrations, the response at lower (and

more relevant) concentrations appears straightforward. Because Raman scattering is a weak, or low-frequency, phenomenon, however, measures of Raman intensity are particularly sensitive to small variations in experimental conditions. The strategy of using an internal comparison to account for Raman independent factors, used above to correct for confounding effects of CNT absorption, can also be employed to mitigate inter-measure variance. Normalizing raw intensity measures to internal standards of known concentration (in this case, surfactant) corrects for some of the non-Raman causes of variance in measured intensity.

Figure 2 shows raw Raman intensity values for 1% Pl-F127 (aq) suspensions with varying concentrations of MWCNTs (2–10 μg/ml). Shown are data for the CNT 'D' peaks (at 1309 cm^{-1}) and the surfactant peaks at 1450 cm^{-1} (Corresponding data for the 'G' peak at 1620 cm^{-1} in Fig. S1 in the Supplementary data, available at *Annals of Occupational Hygiene* online). While the correlation between 'D' peak scattering intensity and

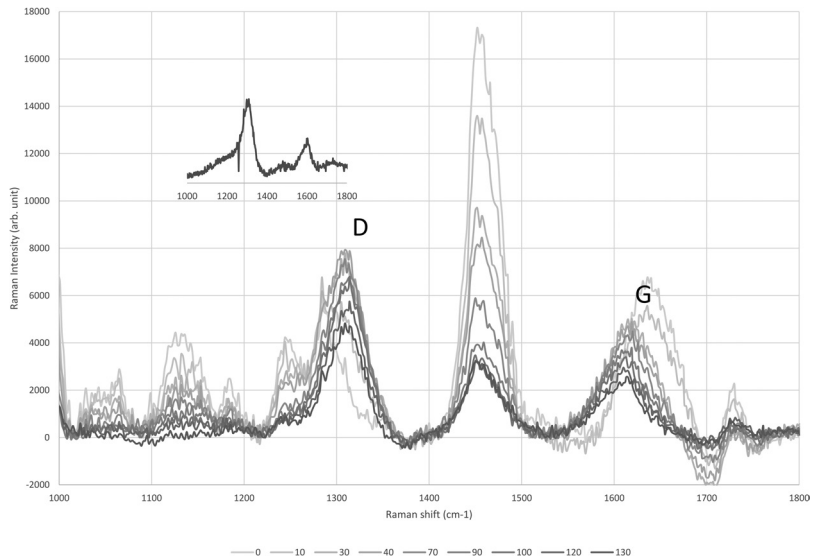

Figure 1. Raman spectra of Baytubes 150 HP MWCNTs in 1% Pl-127 (aq) at CNT concentrations of: 0, 10, 30, 40, 70, 90, 100, 120, and 130 μg/ml. Spectrum of bulk Baytubes 150 HP MWCNTs inset.

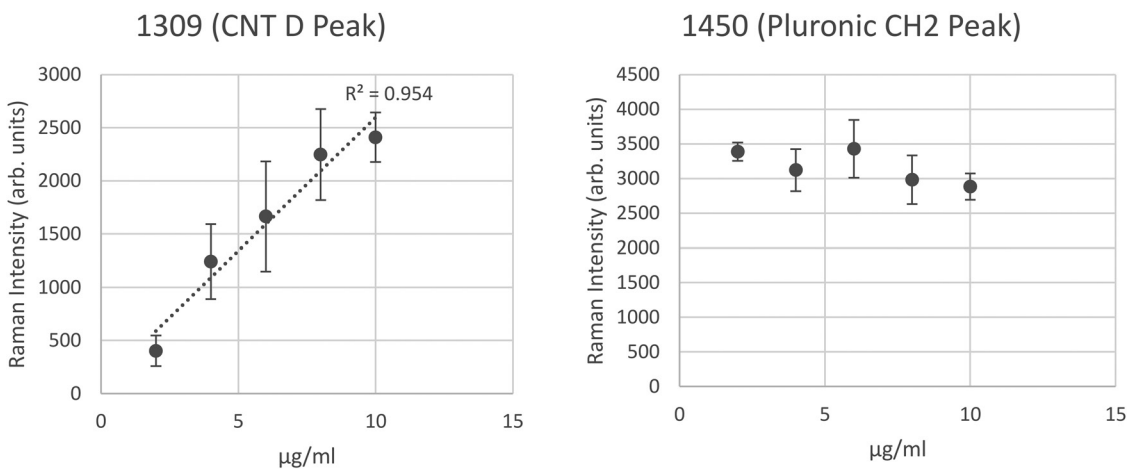

Figure 2. The 1309 cm^{-1} (CNT 'D' peak) and 1450 cm^{-1} (surfactant peak) Raman shifts of Baytubes 150 HP MWCNTs in 1% Pl-127 (aq) at concentrations of: 2, 4, 6, 8, and 10 μg/ml, in 1 cm pathlength quartz cuvettes. Error bars represent standard error over three measurements.

CNT concentration is apparent, the high standard error makes it difficult to use the relationship for estimates of concentration without a high degree of uncertainty. However, when normalizing each 'D' peak measure to a surfactant peak (whose concentration is known and constant), error was significantly reduced (Fig. 3). Among the sources of error that may have been mitigated to improve precision are as follows: small changes in experiment geometry due to sample positioning; changes in excitation due to laser drift; localized sample degradation caused by excitation, and; shifts in ambient conditions, especially light.

As discussed, at higher CNT concentrations (>100 μg CNTs ml^{-1}), analysis is complicated by CNT absorption. In practice, this limitation may be a minor concern because airborne CNT concentrations in occupational settings are generally low (e.g. under 10 μg m^{-1})(Dahm *et al.*, 2015), and measurement of higher concentrations can be performed on dilutions. However, the sensitivity of Raman intensity to confounding variables, affecting analytical precision, is an obstacle with broader implications, especially if the method is to be of general use (across locations and instruments) at low concentrations, where inter-measure variability may preclude accurate quantification at levels approaching the REL of 1 μg m^{-1}. To present samples in a more uniform manner, suspensions were analyzed in glass capillary tubes, but these results also have high variability (Fig. S2 in the Supplementary data, available at *Annals of Occupational Hygiene* online). Also, although stable CNT suspensions can be maintained long enough for measurements, complete suspension of a bulk sample can be difficult, and both the degree of dispersion and tendency for a given CNT material to re-agglomerate can be sample dependent. Thus, use of bulk materials for calibration would likely require prior size segregation when a material contains large agglomerates.

Quantification of CNTs on filters by Raman mapping

Starting from random points, we mapped defined areas of quartz-fiber filters by raster scanning, evaluating each point by Raman for the presence of CNT peaks, returning either a positive or negative result. For each filter, three 0.16 mm^2 Raman maps were produced (Figs S3 and S4 in the Supplementary data, available at *Annals of Occupational Hygiene* online). The total area mapped (0.48 mm^2) for each 25-mm filter represents ~0.1% of the total sample collection area (~415 mm^2). The number of surveyed areas at which CNTs were present was determined by a peak identification algorithm (Gui *et al.* 2007).

Mapping results for two laboratory-generated CNT air samples collected on quartz-fiber filters at different filter loadings are shown in Fig. 4, which shows a comparison of the results of the mapping data with the total EC collected on the filter surface. A correlation (R^2 = 0.83 and 0.95) between CNT map counts (map points at which CNTs were detected) and mass is apparent. At these loadings, imprecision in the mapping data makes an accurate characterization of the correlation difficult. This measurement variance is likely the combined result of the non-uniformity of the sample distribution across the filter relative to the small portion of the total area mapped. Calculated as three times the error of the linear regression, divided by the slope, the LODs for the mapping data are 13 and 9 μg EC on filter for the SWeNT and Arkema samples, respectively.

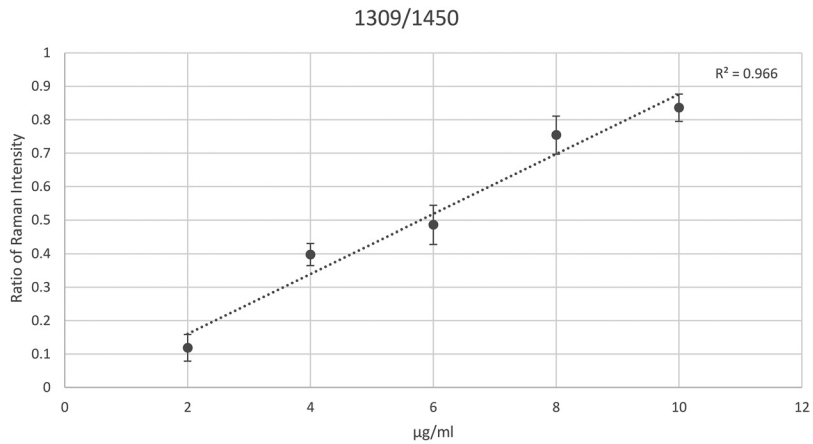

Figure 3. Ratio of the 1309 cm^{-1} (CNT 'D' peak) to the 1450 cm^{-1} (surfactant peak) Raman shift of Baytubes 150 HP MWCNTs in 1% PI-127 (aq) at concentrations of: 2, 4, 6, 8, and 10 μg/ml. Error bars represent standard error over three measurements.

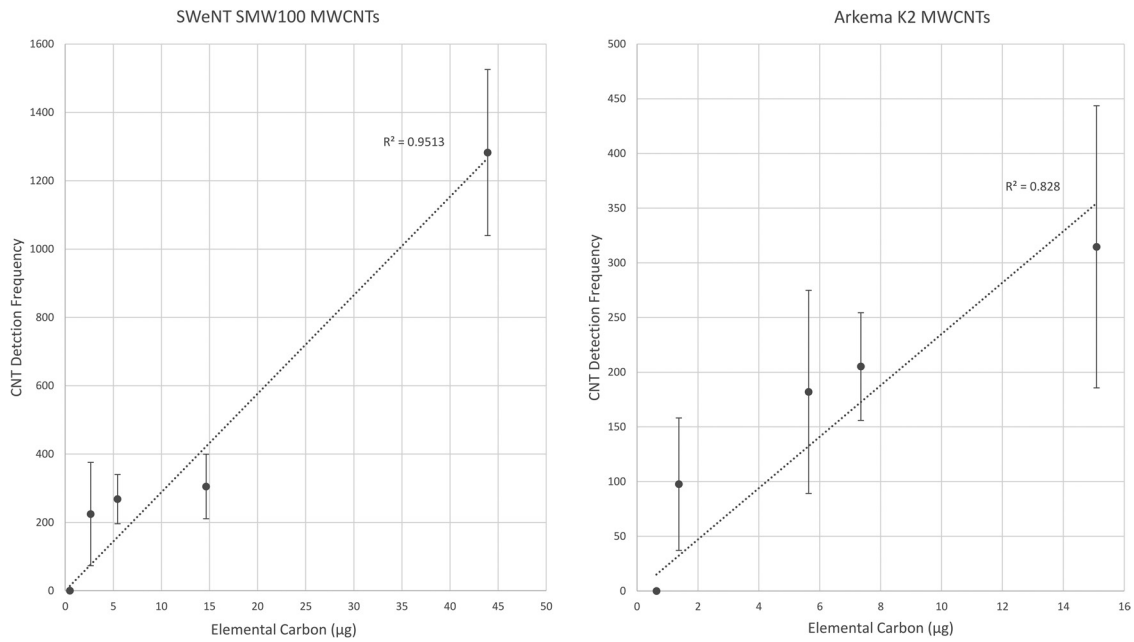

Figure 4. Detection frequency of two multi-walled carbon nanotube aerosol samples collected on 25-mm quartz-fiber filters at different filter loadings (total elemental carbon on filter shown). Mean of three 0.16 mm² maps is shown, along with standard error.

Although it may be possible to generate more homogeneous sample distributions on 25-mm filters under controlled conditions, it may not be realistic to expect real-world samples to conform to such a requirement. The relative portion of the collection area that can be mapped, however, is under our control (within certain practical limits—time, primarily). To improve the fidelity of the mapping measurement, and lower the LOD, we examined samples with a greatly reduced deposit area, while retaining approximately the same range of surface mass densities. In practice, we had envisioned sample deposition as a small spot (e.g. several mm diameter), either using a sample suspension applied as a well-defined deposit or by direct collection on a filter/substrate. The small deposit allowed measurement of a substantially higher proportion of the sample area when using a mapping procedure identical to that described above, while requiring collection of less total analyte mass. Similar approaches were recently reported for determination of silica (Stacey *et al.* 2017) and soot (Grafen *et al.*, 2015) at low levels by Raman mapping.

To reduce the deposit area, suspensions of 6-Helix SWCNTs (Helix) in Pl F127 surfactant solution were prepared at various concentrations and aliquoted (2 µl) directly onto the surface of quartz-fiber filters. The area of the sample deposit was ~5 mm². Again, three Raman maps were produced for the sample deposit, each with an area of 0.16 mm². Although each mapping measurement began at a random location within the sample area, because of the much smaller sample area, it is far more likely than in the previous experiments that the mapped areas may overlap, but this possibility was not considered. Assuming no overlap, the total mapped area of 0.48 mm² represents ~9.8% of the total sample area.

Figure 5 shows the correlation between the mapping data and the estimated total EC mass on the filter. Uncertainty in the slope, 3.02 ± 0.28, is much lower than that obtained in the mapping measurements on the 25-mm filters: 28.8 ± 7.3 (SWeNT) and 23.5 ± 13 (Arkema) (Fig. 4). This anticipated increase in precision, attributable to the approximately two orders of magnitude increase in map coverage (from 0.1 to 9.8%), is apparent. The LOD calculated from the trend line is 52 ng, and 176 ng total EC (on filter) is the limit of quantification.

As in the case of CNT suspensions, the degree of agglomeration, affecting the uniformity of the mass distribution, is also a factor in the measurement by Raman mapping of filter samples of CNTs. An increase in sampling deposit density can mitigate this effect, but there are practical constraints (primarily time) that may limit the thoroughness of the mapping. For field applications, the differential effects of agglomeration on signal response may necessitate construction of calibration

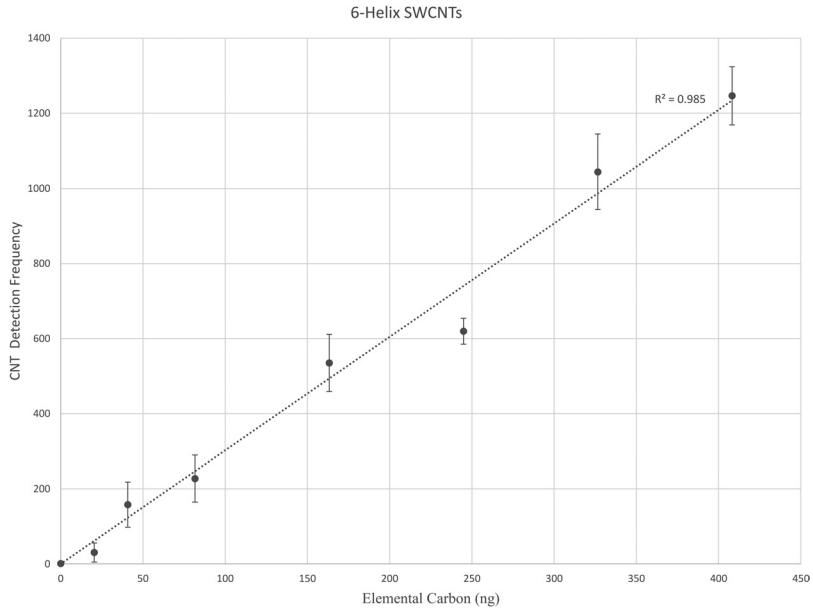

Figure 5. Raman peak detection frequency of a single-walled carbon nanotube sample in surfactant solution deposited on quartz-fiber filters by micropipette (approximate area 0.05 cm^2). Mean of three 0.16 mm^2 maps is shown, with standard error.

curves for different materials. Larger (non-respirable) particle agglomerates are a source of variability, but these can be excluded from the air samples by use of an aerosol pre-classifier upstream of the sample filter, to select the respirable fraction. Respirable aerosol particles normally deposit more evenly across the filter than do larger particles, improving the mapping precision. As discussed, precision also can be improved by increasing the area mapped relative to the total sample area. Reducing the collection area enables practical interrogation of larger portion of the filter, to further increase precision and lower the LOD to a level necessary for exposure assessment at low concentrations (e.g. near the NIOSH REL of 1 μg EC/m^3).

Conclusions

Raman analysis as a means of identifying and quantifying CNTs has the virtues of speed, simplicity, and relatively low cost. We examined two methods by which Raman analysis might be employed to evaluate samples for the presence of CNTs: through analysis of CNT suspensions in surfactant solutions, and by direct Raman mapping of filter deposits. Suspensions were examined to determine whether collection in a dispersant for direct analysis was feasible, and because focused deposition of a liquid-based sample (e.g. resuspension of a filter sample) can allow identification and quantification of CNTs at much lower LODs. In addition, suspensions provided a convenient means to prepare small-area samples. Similar deposits also could be obtained on filters/substrates through air sampling. Although liquid- and filter-based samples both have limitations—some common to Raman measurements, and some particular to CNT measurements—correlations between the Raman results and EC mass were found. In particular, the Raman mapping method for small-area deposits shows promise for quantification of airborne CNTs at levels relevant to occupational monitoring.

The advantages of Raman mapping as a quantitative technique consist in combining the qualitative capabilities of Raman with a more reliable method of particle quantitation than measuring Raman intensity. Further development of the method requires application to complex mixtures, but Raman analysis of mixtures is a well-developed field. In principle, a Raman mapping method for measuring workplace CNTs could be successfully applied to the analysis of real-world samples. However, concentration of samples into small areas may be required for field detection at low levels, e.g., at or below the NIOSH REL of 1 μg m^{-1}. At 2 lpm, collection of air samples at the REL could produce EC masses measurable by this technique (~50 ng) in as few as 25 min. The method also has utility as a qualitative screening tool to identify graphitic carbon, indicating the presence and relative amounts of CNTs in samples (air and surface) from workplaces that produce/process CNT materials.

Supplementary Data

Supplementary data are available at *Annals of Work Exposures and Health* online.

Declaration

Funding for this project was provided by the National Institute for Occupational Safety and Health. The findings and conclusions in this report are those of the authors and do not necessarily represent the views of the National Institute for Occupational Safety and Health. Mention of product or company name does not constitute endorsement by the Centers for Disease Control and Prevention.

Conflict of Interest

None declared.

References

Aschberger K, Johnston HJ, Stone V *et al.* (2010) Review of carbon nanotubes toxicity and exposure–appraisal of human health risk assessment based on open literature. *Crit Rev Toxicol*; **40**: 759–90.

van Berlo D, Wilhelmi V, Boots AW *et al.* (2014) Apoptotic, inflammatory, and fibrogenic effects of two different types of multi-walled carbon nanotubes in mouse lung. *Arch Toxicol*; **88**: 1725–37.

Birch, ME. (2016) *Monitoring diesel exhaust in the workplace. NIOSH Manual of Analytical Methods (NMAM)*, 5th edn, Chapter DL, DHHS, CDC, National Institute for Occupational Safety and Health (NIOSH), 28 June 2016, http://www.cdc.gov/niosh/nmam/chapters.html. Accessed May 2017.

Birch ME, Cary RA. (1996) Elemental carbon-based method for monitoring occupational exposures to particulate diesel exhaust. *Aerosol Sci Technol*; **25**: 221–41.

Birch ME, Wang C, Fernback JH *et al.* (2016a) *Analysis of carbon nanotubes and nanofibers on mixed cellulose ester filters by transmission electron microscopy. NIOSH Manual of Analytical Methods (NMAM)*. 5th edn. Cincinnati, OH: U.S. Department of Health and Human Services, Centers for Disease Control and Prevention, National Institute for Occupational Safety and Health, DHHS (NIOSH). Under review for publication at: http://www.cdc.gov/niosh/nmam/. Accessed May 2017.

Birch ME, Wang C, Fernback JH *et al.* (2016b) *Workplace monitoring of airborne carbon nanomaterials by HRTEM*. Proceedings of the Microscopy and Microanalysis conference, Columbus, OH, July 24–28, 2016.

Dahm MM, Schubauer-Berigan MK, Evans DE *et al.* (2015) Carbon nanotube and nanofiber exposure assessments: an analysis of 14 site visits. *Ann Occup Hyg*; **59**: 705–23.

Dresselhaus MS, Dresselhaus G, Saito R *et al.* (2005) Raman spectroscopy of carbon nanotubes. *Physics Reports*; **409**: 47–99.

Graf D, Molitor F, Ensslin K *et al.* (2007) Raman imaging of graphene. *Solid State Commun*; **143**: 44–6.

Grafen M, Nalpantidis K, Platte F *et al.* (2015) Multivariate characterization of a continuous soot monitoring system based on Raman spectroscopy. *Aerosol Sci Technol*; **49**: 997–1008.

Grosse Y, Loomis D, Guyton KZ *et al.*; International Agency for Research on Cancer Monograph Working Group. (2014) Carcinogenicity of fluoro-edenite, silicon carbide fibres and whiskers, and carbon nanotubes. *Lancet Oncol*; **15**: 1427–8.

Gui EL, Li LJ, Zhang K *et al.* (2007) DNA sensing by field-effect transistors based on networks of carbon nanotubes. *J Am Chem Soc*; **129**: 14427–32.

Hoang VD. (2014) Wavelet-based spectral analysis. *Trends Analyt Chem*; **62**: 144–53.

International Agency for Research on Cancer (IARC). (2014) *Fluoro-edenite, silicon carbide fibres and whiskers, and single-walled and multi-walled carbon nanotubes*. Vol. **111**. Lyon, France: IARC Working Group. IARC Monogr Eval Carcinog Risk Chem Hum.

Irurzun VM, Ruiz MP, Resasco DE. (2010) Raman intensity measurements of single-walled carbon nanotube suspensions as a quantitative technique to assess purity. *Carbon*; **48**: 2873–81.

Ku BK, Emery MS, Maynard AD *et al.* (2006) In situ structure characterization of airborne carbon nanofibres by a tandem mobility-mass analysis. *Nanotechnology*; **17**: 3613–21.

Lam CW, James JT, McCluskey R *et al.* (2004) Pulmonary toxicity of single-wall carbon nanotubes in mice 7 and 90 days after intratracheal instillation. *Toxicol Sci*; **77**: 126–34.

Lam CW, James JT, McCluskey R *et al.* (2006) A review of carbon nanotube toxicity and assessment of potential occupational and environmental health risks. *Crit Rev Toxicol*; **36**: 189–217.

Li S, Nyagilo JO, Dave DP *et al.* (2013) Continuous wavelet transform based partial least squares regression for quantitative analysis of Raman spectrum. *IEEE Trans Nanobioscience*; **12**: 214–21.

López-Lorente AI, Simonet BM, Valcárcel M. (2013) Qualitative detection and quantitative determination of single-walled carbon nanotubes in mixtures of carbon nanotubes with a portable Raman spectrometer. *Analyst*; **138**: 2378–85.

Ma-Hock L, Treumann S, Strauss V *et al.* (2009) Inhalation toxicity of multiwall carbon nanotubes in rats exposed for 3 months. *Toxicol Sci*; **112**: 468–81.

National Institute for Occupational Safety and Health. (2003) *Diesel particulate matter (as elemental carbon): Method 5040 (supplement issued 3/15/03), NIOSH manual of analytical methods*. 4th edn, Cincinnati, OH: U.S. Department of Health and Human Services, Public Health Service, Centers for Disease Control and Prevention, National Institute for Occupational Safety and Health, DHHS (NIOSH) Publication No. 94-113.

National Institute for Occupational Safety and Health. (2013) *Current intelligence bulletin 65: occupational exposure to carbon nanotubes and nanofibers*. U.S. Department of Health and Human Services, Public Health Service, Centers for Disease Control and Prevention, National Institute for Occupational Safety and Health, DHHS Publication 2013-145.

Porter DW, Hubbs AF, Chen BT *et al.* (2013) Acute pulmonary dose-responses to inhaled multi-walled carbon nanotubes. *Nanotoxicology*; **7**: 1179–94.

Ruedi B. (2016) Device for measuring the exposure to small particles, in particular nanotubes, *WIPO Application WO2016EP56329 20160323*, 2016.

Rydman EM, Ilves M, Vanhala E *et al.* (2015) A single aspiration of rod-like carbon nanotubes induces asbestos-like pulmonary inflammation mediated in part by the IL-1 receptor. *Toxicol Sci*; **147**: 140–55.

Salzmann CG, Chu BT, Tobias G *et al.* (2007) Quantitative assessment of carbon nanotube dispersions by Raman spectroscopy. *Carbon*; **45**: 907–12.

Sargent LM, Porter DW, Staska LM *et al.* (2014) Promotion of lung adenocarcinoma following inhalation exposure to multi-walled carbon nanotubes. *Part Fibre Toxicol*; **11**: 3.

Shin K, Chung H. (2013) Wide area coverage Raman spectroscopy for reliable quantitative analysis and its applications. *Analyst*; **138**: 3335–46.

Shvedova AA, Kisin E, Murray AR *et al.* (2008) Inhalation vs. aspiration of single-walled carbon nanotubes in C57BL/6 mice: inflammation, fibrosis, oxidative stress, and mutagenesis. *Am J Physiol Lung Cell Mol Physiol*; **295**: L552–65.

Stacey P, Mader KT, Sammon C. (2017) Feasibility of the quantification of respirable crystalline silica by mass on aerosol sampling filters using Raman microscopy. *J. Raman Spectrosc*; **48**: 720–25.

Zhang ZM, Chen S, Liang YZ. (2010) An intelligent background-correction algorithm for highly fluorescent samples in Raman spectroscopy. *J. Raman Spectrosc*; **41**: 659.